




Article

5-Hydroxymethylfurfural and Furfural Base-Free Oxidation over AuPd Embedded Bimetallic Nanoparticles

Camila P. Ferraz ^{1,2}, Natalia J. S. Costa ¹, Erico Teixeira-Neto ³, Ângela A. Teixeira-Neto ³, Cleber W. Liria ⁴, Joëlle Thuriot-Roukos ², M. Teresa Machini ⁴ , Rénato Froidevaux ⁵, Franck Dumeignil ² , Liane M. Rossi ¹ and Robert Wojcieszak ^{2,*} 

¹ Departamento de Química Fundamental, Instituto de Química, Universidade de São Paulo, São Paulo 05508-000, Brazil; camila.ferraz@univ-lille.fr (C.P.F.); nataliajcosta@gmail.com (N.J.S.C.); lrossi@iq.usp.br (L.M.R.)

² Univ.Lille, CNRS, Centrale Lille, ENSCL, Univ.Artois, UMR 8181—UCCS—Unité de Catalyse et Chimie du Solide, F-59000 Lille, France; joelle.thuriot@univ-lille.fr (J.T.-R.); franck.dumeignil@univ-lille.fr (F.D.)

³ Laboratório de Microscopia Eletrônica, LNNano-CNPEM, C.P. 6192, Campinas 13083-970, Brazil; erico.teixeira.neto@gmail.com (E.T.-N.); angelaalb@gmail.com (Â.A.T.-N.)

⁴ Departamento de Bioquímica, Instituto de Química, Universidade de São Paulo, São Paulo 05508-000, Brazil; cwliria@iq.usp.br (C.W.L.); mtmachini@iq.usp.br (M.T.M.)

⁵ Univ.Lille, INRA, ISA, University Artois, Univ.Littoral Côte d'Opale, EA 7394—ICV—Institute Charles Viollette, F-59000 Lille, France; renato.froidevaux@univ-lille.fr

* Correspondence: robert.wojcieszak@univ-lille1.fr

Received: 4 December 2019; Accepted: 2 January 2020; Published: 4 January 2020



Abstract: The heterogeneous catalytic partial oxidation of alcohols and aldehydes in the liquid phase usually needs the addition of a homogeneous base, which in turn makes the products' recovery cumbersome, and can further induce undesired side reactions. In the present work, we propose the use of novel catalysts based on metallic Au, Pd and bimetallic AuPd nanoparticles embedded in a titanosilicate matrix. The as-prepared catalysts showed good efficiency in the base-free partial oxidation of furfural and 5-hydroxymethylfurfural. Au₄Pd₁@SiTi catalyst showed high selectivity (78%) to monoacids (namely, 5-formyl-2-furancarboxylic acid and 5-hydroxymethyl-2-furancarboxylic acid) at 50% 5-hydroxymethylfurfural (HMF) conversion. The selectivity even reached 83% in the case of furfural oxidation to furoic acid (at 50% furfural conversion). The performances of the catalysts strongly depended on the Au–Pd ratio, with an optimal value of 4:1. The pH of the solution was always below 3.5 and no leaching of metals was observed, confirming the stabilization of the metal nanoparticles within the titanosilicate host matrix.

Keywords: bimetallic nanoparticles; base-free; green oxidation; embedded catalysts; biomass

1. Introduction

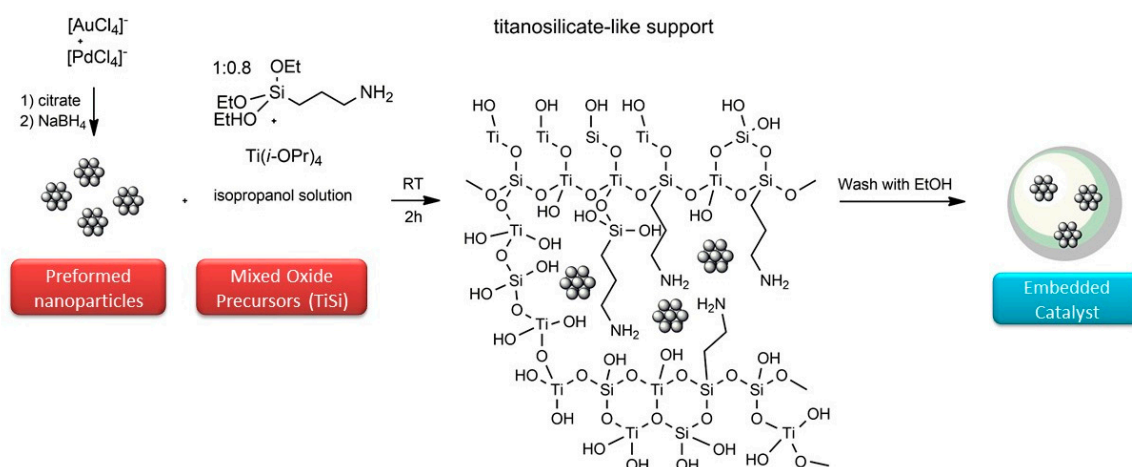
5-hydroxymethylfurfural (HMF) is one of the top 12 highly valued compounds identified early as promising platform molecules within the frame of the development of biorefineries [1–4]. HMF is readily obtained by the dehydration of glucose and through the intermediate isomerization of fructose, the glucose being potentially obtained by cellulose hydrolysis [2,4]. The shared enthusiasm around HMF lies in its great versatility in enabling the production of a wide variety of fuels and high value-added chemicals [2,4,5]. In particular, the products obtained via partial oxidation processes are of high interest for the chemical and polymer industries. Such derivatives have the potential to replace petrochemical-based monomers [2,6]. Indeed, 2,5-furandicarboxylic acid (FDCA), for example,

is used for the synthesis of polyethylene furoate (PEF), which is a promising alternative to polyethylene terephthalate (PET). In addition to being a green alternative, PEF does not bio-accumulate and is biodegradable [6].

Like HMF, furfural is also attracting much attention. It is also part as of the aforementioned highly valued compounds list, with a very high potential for biorefineries development [1–4,7]. It is generally obtained from hemicellulose, mainly via the hydrolysis of xylose polymers and subsequent dehydration. The partial oxidation of furfural gives furoic acid (furan-2-carboxylic acid), which has various applications in the agrochemical, flavor, pharmaceutical, and fine chemistry industries.

HMF and furfural oxidation reactions can be carried out using different methods, including chemical oxidation, biochemical transformation and homogeneous or heterogeneous catalytic conversions [8–10]. However, there are still several drawbacks related to the difficulties in the control of undesired side product formation and the final separation step. Moreover, very often, the oxidation is carried out in the presence of an inorganic base, such as NaOH or KOH. Basic media can be responsible for HMF and furfural degradation. Indeed, placing HMF or furfural under high pH conditions in the absence of a catalyst yields high substrate conversion, but without the formation of the desired oxidation products. The formation of a black precipitate-like compound is frequently observed, which is attributed to the formation of humins [11–14]. A high pH of the medium also favors the formation of low molar weight acids such as levulinic acid and formic acid, consecutively to C–C bond cleavage. Previous studies [12–14] show that the challenge in developing catalysts for furfural and HMF partial oxidation lies in the design of heterogeneous catalytic systems capable of maintaining high activity and selectivity while getting rid of the use of a homogeneous base. Regarding Au catalysts, strategies to prevent the use of a base consist of adopting a basic and/or nanometric support and/or adding a second metal (bimetallic). In the latter case, Au with high selectivity forms bimetallic nanomaterials that can combine the advantages of different components at the atomic level. It can also increase catalytic activity and stability in oxidation reactions of organic compounds in water [15,16]. Therefore, the development of a titanasilicate support in which Au, Pd and bimetallic AuPd nanoparticles are encapsulated should increase the stability of the catalysts while preventing leaching of the metal.

Herein, we report a study of embedded catalysts for base-free furfural and HMF partial oxidation. Novel $\text{Au}_x\text{Pd}_y\text{@SiTi}$ nanomaterials were developed, where the AuPd nanoparticles were embedded in a titanasilicate matrix (Scheme 1). Different Au–Pd ratios were used in order to optimize base-free furfural and HMF partial oxidation to the desired compounds.



Scheme 1. Schematic representation of the synthesis procedure.

2. Results

In this work, two different oxidation reactions were studied. The $\text{Au}_x\text{Pd}_y\text{@SiTi}$ systems were first used in HMF oxidation to identify/optimize the main factors governing the activity of bimetallic AuPd nanoparticles during the base-free oxidation reaction in water using O_2 as oxidant. Au@SiTi and Pd@SiTi monometallic catalysts were also developed to understand the effect of AuPd's alloying activity by comparison with their bimetallic counterparts (Figure 1). The Au–Pd ratio was varied in bimetallic catalysts from $\text{Au}_4\text{Pd}_1\text{@SiTi}$ to $\text{Au}_1\text{Pd}_4\text{@SiTi}$, and the effect of Au or Pd enrichment in the alloy on catalysis activity and selectivity was evaluated. In addition, the corresponding supported versions of the embedded catalysts, denoted as $\text{Au}_4\text{Pd}_1/\text{SiTi}$, $\text{Au}_1\text{Pd}_1/\text{SiTi}$ and $\text{Au}_1\text{Pd}_4/\text{SiTi}$, were also synthesized for comparison (Figure 1).

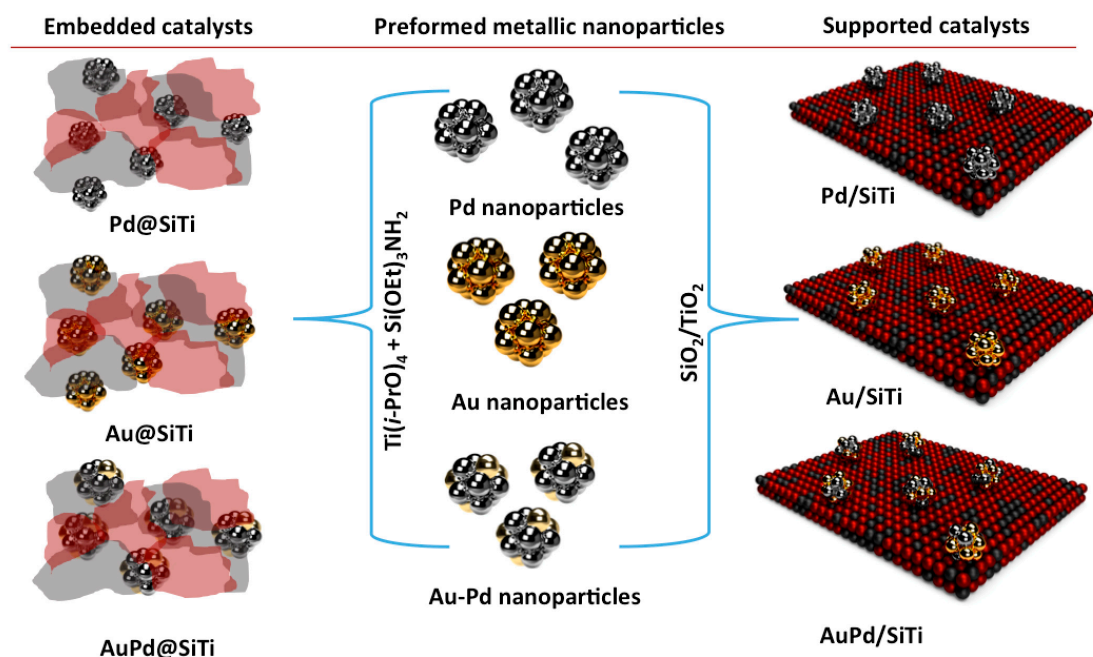


Figure 1. Schematic representation of the compared catalytic systems. Embedded catalysts are denoted as $\text{Au}_x\text{Pd}_y\text{@SiTi}$ and supported catalysts as $\text{Au}_x\text{Pd}_y/\text{SiTi}$ (red— TiO_2 , gray— SiO_2).

Initially, AuPd equimolar catalyst was synthesized, characterized and evaluated. $\text{Au}_1\text{Pd}_1\text{@SiTi}$ with Au–Pd molar ratio of 1 was prepared using equivalent quantities of APTES and TIP (500 mg) for comparison to its monometallic counterparts (Au@SiTi and Pd@SiTi). The catalysts were prepared using preformed NPs, which were stabilized by sodium citrate and reduced by NaBH_4 in a well-known and reproducible method [17] to provide Au, Pd and AuPd nanoparticles of about 4 nm. The as-prepared nanoparticles were then soaked in a mixed titanasilicate oxide and had their size preserved after immobilization in the support (as represented in Scheme 1). Embedded Au_1Pd_1 nanoparticles were monodispersed with a mean size of 3.8 ± 0.8 nm (Figure 2). Following this, two other catalysts with Au–Pd molar ratios of 4:1 and 1:4 ($\text{Au}_4\text{Pd}_1\text{@SiTi}$ and $\text{Au}_1\text{Pd}_4\text{@SiTi}$, respectively) were synthesized and characterized. In both cases, the mean particle size was again about 4 nm (Figure 2).

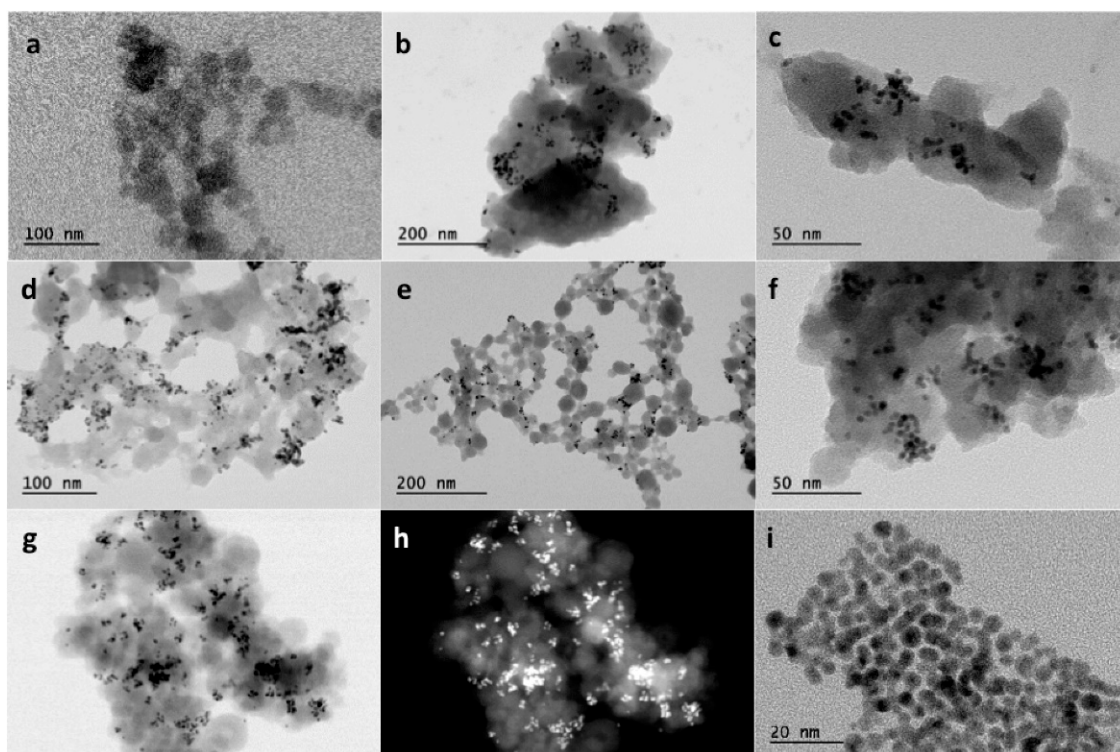


Figure 2. Transmission electron microscopy (TEM) images of (a) bare SiTi; (b) Au@SiTi; (c) Pd@SiTi; (d) Au₄Pd₁@SiTi; (e) Au₁Pd₁@SiTi; (f) Au₁Pd₄@SiTi; (g) Au₁Pd₁@SiTi; (h) Au₁Pd₁@SiTi in dark field measurement and (i) preformed Au₁Pd₁ nanoparticles stabilized by sodium citrate and used for the embedded catalysts synthesis.

Considering the same metal loading (ca. 2.2 wt.%, Table 1) and particle size, the catalytic performances are expected to be governed mainly by the interaction of the metal with the support and by the chemical composition of the bimetallic nanoparticles. The formation of Pd-rich or Au-rich nano alloys can particularly strongly affect the catalytic activity. The Brunauer-Emmett-Teller (BET) analysis showed that different porosities were obtained for the embedded samples. The BET surface area of the Au₄Pd₁@SiTi sample was twice as big as that of Au₁Pd₁ sample (78 and 39 m²/g, respectively). No result was observed for the Pd-rich sample (BET surface area of <1 m²g^{−1}) after being performed twice. This could be due to the collapse of the structure during the degassing step (150 °C) or the complete filling of the pores by the organic precursors.

The high-resolution transmission electron microscopy (TEM) images and Energy Dispersive X-Ray Spectrometry (EDS) analysis of the Au₁Pd₁@SiTi catalyst are shown in Figure 3. This sample was chosen because of the equimolar Au:Pd ratio. It was confirmed that the encapsulation of the bimetallic nanoparticles in SiTi preserved the mean particle size. Moreover, chemical mapping of the images suggested some segregation of Au and Pd in the NPs. A core shell structure with a Pd-rich shell was formed. Regarding the titanosilicate structure, Si and Ti were uniformly distributed in the solid, but Ti seemed to surround the bimetallic nanoparticles (Figure 3).

Table 1. Chemical composition of $\text{Au}_x\text{Pd}_y\text{@SiTi}$ and $\text{Au}_x\text{Pd}_y/\text{SiTi}$ catalysts as determined by inductively coupled plasma optical emission spectrometry (ICP—OES) and X-ray fluorescence spectrometry (XRF) for the former.

Catalyst	Au (%)	Pd (%)	Metal % (Au + Pd)	Si (%)	Ti (%)	Au:Pd ^a	Si:Ti ^b
$\text{Au}_4\text{Pd}_1\text{@SiTi}$	1.68	0.42	2.11	5.02	21.69	79:21 (77:23) 80:20	19:81 (15:85)
$\text{Au}_1\text{Pd}_1\text{@SiTi}$	1.37	0.97	2.34	3.75	20.41	58:42 (50:50) 50:50	16:84 (16:84)
$\text{Au}_1\text{Pd}_4\text{@SiTi}$	0.69	1.60	2.29	4.14	22.08	30:70 (22:78) 20:80	16:84 (17:83)
$\text{Au}_4\text{Pd}_1/\text{SiTi}$	5.41	0.80	6.21	8.83	48.61	78:22 80:20	15:85
$\text{Au}_1\text{Pd}_1/\text{SiTi}$	2.30	1.31	3.61	8.83	48.61	50:50 50:50	15:85
$\text{Au}_1\text{Pd}_4/\text{SiTi}$	1.21	2.21	3.43	8.83	48.61	23:77 20:80	15:85
Au@SiTi	6.40	-	6.40	-	-	-	-
Pd@SiTi	-	3.01	3.01	-	-	-	-
SiTi	-	-	-	8.83	48.61	-	15:85

^a XRF results given in brackets, theoretical ratio in italic; ^b theoretical value of 60:40.

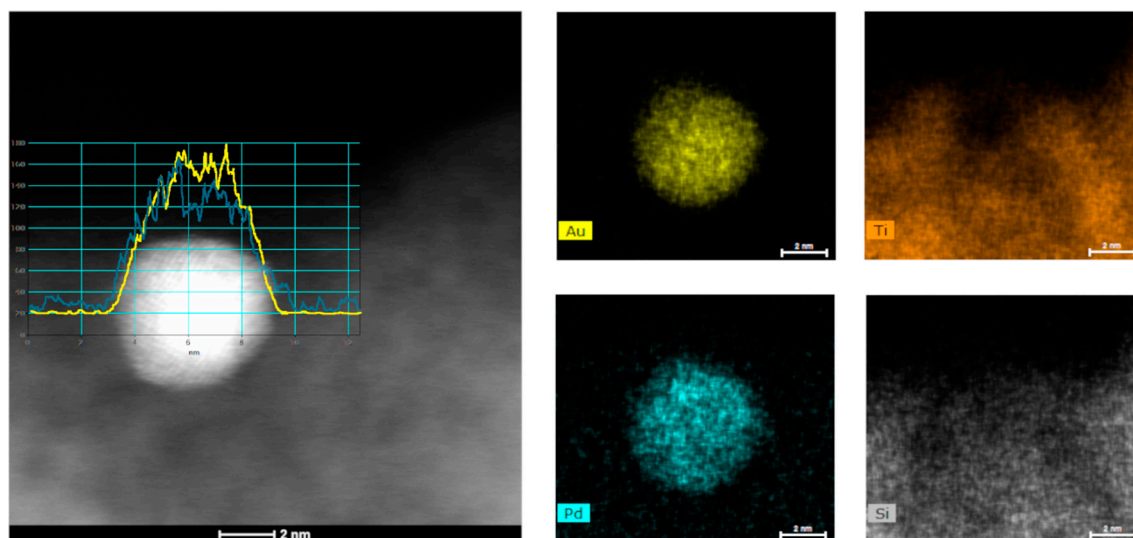


Figure 3. HRTEM HAADF image of the $\text{Au}_1\text{Pd}_1\text{@SiTi}$ catalyst and X-ray mapping of the sample.

All catalysts were characterized by inductively coupled plasma optical emission spectrometry (ICP—OES) to determine their Au, Pd, Si and Ti contents (Table 1). The Au–Pd ratios for the catalysts were reasonably consistent with the expected values, resulting in catalysts with about 2.2 wt.% of metal loading (for embedded catalysts). Higher amounts of metals were obtained for the supported $\text{Au}_1\text{Pd}_1/\text{SiTi}$ and $\text{Au}_1\text{Pd}_4/\text{SiTi}$ samples (about 3.3 wt.%). In the case of the $\text{Au}_4\text{Pd}_1/\text{SiTi}$ sample, the metal loading reached 6 wt.% (Table 1). In all cases, the Ti–Si ratio was close to 4.

X-ray photoelectron spectroscopy (XPS) analysis confirmed that AuPd nanoparticles were embedded in the Si–Ti matrix. The results can be seen in the Table 2 below. It can be clearly observed the strong decrease in the Au and Pd content for the embedded samples as compared to the corresponding supported catalysts. This can be explained by the covering of the metal nanoparticles with the oxide phases.

Table 2. X-ray photoelectron spectroscopy (XPS) analysis of the supported and embedded catalysts.

	Au at%	Pd at%	Au/Pd mol	Pd0/PdII
Au ₁ Pd ₁ /SiTi	47 ± 1	24.0 ± 0.7	1.05 ± 0.01	4 ± 1
Au ₁ Pd ₁ @TiSi	6.4 ± 0.2	3.5 ± 0.2	1.00 ± 0.09	2.2 ± 0.2
Au ₁ Pd ₄ /SiTi	24 ± 1	42.4 ± 0.8	0.31 ± 0.02	2.4 ± 0.2
Au ₁ Pd ₄ @SiTi	2.2 ± 0.1	5.1 ± 0.1	0.24 ± 0.01	2.7 ± 0.5
Au ₄ Pd ₁ /SiTi	61 ± 1	9.7 ± 0.1	3.40 ± 0.03	3.8 ± 0.4
Au ₄ Pd ₁ @SiTi	9.4 ± 0.3	1.3 ± 0.03	3.95 ± 0.06	3.5 ± 0.8

A good accordance between the surface (XPS) and bulk analyses (XRF, ICP) was observed in term of chemical composition. As can be seen from Tables 1 and 2, the molar ratio between both metals is similar for all techniques used. This could be explained by the homogeneous composition of the bimetallic nanoparticles.

The solids had Ti contents much higher than expected (theoretical Si–Ti value of 60:40), thus with relatively low amounts of Si (actual average Si–Ti ratio of 15:85). Under these conditions, the hydrolysis of the precursors may not be complete; in particular, APTES (silica precursor) could remain in the solution, which explains the higher Ti content as compared to the expected ones and also the fact that the Si–Ti ratio is the same for all the synthesized embedded samples. The catalysts were also characterized by XRF analysis (Table 1), and the Au–Pd and Si–Ti ratios were found the same as those obtained by ICP-OES. The XRF values were closer to the theoretical ones. The Au–Pd molar ratios of 4:1, 1:1 and 1:4 were confirmed by ICP and XRF analyses.

2.1. HMF Oxidation

Effect of Au:Pd Ratio on Catalytic Activity

The results of HMF oxidation are presented in Figures 4 and 5, and, as expected, all the catalysts were active. Variation in the AuPd composition affected both conversions and selectivities, with better catalysts being obtained when the Au proportion was increased in the bimetallic systems (Figure 4a). A volcano profile was observed when plotting the conversion observed after 24 h as a function of the catalysts' composition (Figure 4b), where a maximum activity was reached for the Au₄Pd₁ gold-rich composition. The distribution of the products was also greatly affected by the composition variation (Figure 5). Pure Au favors the formation and accumulation of 5-hydroxymethyl-2-furancarboxylic acid (HFCA), as already observed in a previous study focused on Au catalysts in different supports [18]. The addition of Pd makes possible the formation of 2,5-diformylfuran (FDC) by the chemisorption of HMF via the aldehyde group [19], which was detected in all AuPd (Figure 5b) and pure Pd compositions (Figure 5c). In the Au-rich Au₄Pd₁ composition, the formed FDC was quickly consumed, leading to higher yields of furandicarboxylic acid (FDCA) (Figure 5).

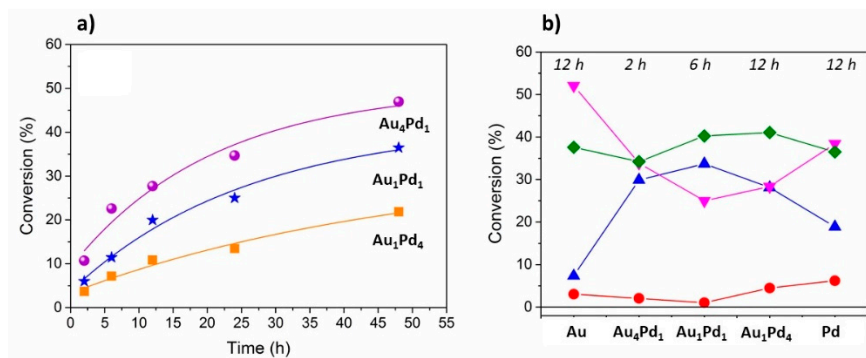


Figure 4. 5-hydroxymethylfurfural (HMF) oxidation in the aqueous phase in the absence of base using Au_xPd_y@SiTi catalysts: conversion and selectivity as a function of time (a), and as a function of Au_xPd_y composition at *iso*-conversion of 10% (b): selectivity to: ● 2-, 5-furandicarboxylic acid (FDCA), ▲ 2, 5-diformylfuran (FDC), ▼ 5-hydroxymethyl-2-furancarboxylic acid HFCA, ◆ 5-formyl-2-furancarboxylic acid (FFCA). Aqueous solution of HMF (30 μmol), substrate/metal = 18 (mol/mol), O₂ (1 bar), 100 °C, 600 rpm.

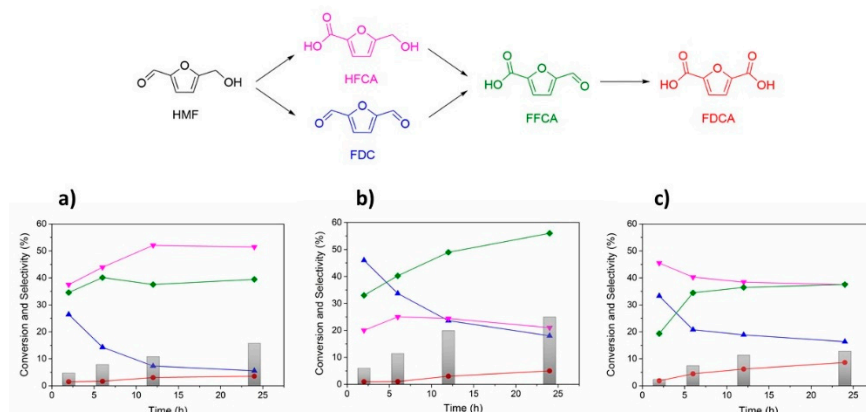


Figure 5. HMF oxidation in the aqueous phase in the absence of base using Au_xPd_y@SiTi catalysts: conversion and selectivity as a function of time: (a) Au@SiTi, (b) Au₁Pd₁@SiTi, (c) Pd@SiTi; selectivity to: ● FDCA, ▲ FDC, ▼ HFCA, ◆ FFCA. Aqueous solution of HMF (30 μmol), substrate/metal = 18 (mol/mol), O₂ (1 bar), 100 °C, 600 rpm.

The activity of the embedded catalysts was compared to that of corresponding supported conventional materials (Table 3). Au/TiO₂ and Au/ZrO₂ catalysts were also studied for comparison (Table 3, Entries 8 and 9).

Table 3. Oxidation of HMF in the aqueous phase in the absence of base for 24 h using embedded Au_xPd_y@SiTi and supported Au_xPd_y/SiTi catalysts. Aqueous solution of HMF (30 μmol), substrate/metal = 18 (mol/mol), O₂ (1 bar), 100 °C, 600 rpm, ^a sample calcined at 500 °C.

Entry	Catalyst	C Balance	S _{FDCA} %	X%	Y _{FDCA} %	TON
1	Au ₄ Pd ₁ @SiTi	74	22	35	8	67
2	Au ₁ Pd ₁ @SiTi	86	5	25	2	65
3	Au ₁ Pd ₄ @SiTi	88	4	14	1	38
4	Au ₄ Pd ₁ /SiTi	74	1	13	<1	43
5	Au ₁ Pd ₁ /SiTi	88	1	6	<1	19
6	Au ₁ Pd ₄ /SiTi	94	6	5	<1	11
7	Au ₁ Pd ₁ PVA@SiTi	78	3	27	1	38
8	Au@SiTi	12	4	16	<1	35
9	Pd@SiTi	16	8	13	<1	32
10 ^a	Au ₄ Pd ₁ @SiTi _{cal}	80	1	11	1	21

The conversion of HMF observed for the embedded samples after 24 h (Table 3, Entries 1–3) was strongly influenced by the composition of the bimetallic nanoparticles. The maximum level of conversion was obtained for the rich gold sample ($\text{Au}_4\text{Pd}_1@\text{SiTi}$) and the lowest for the Pd-rich sample ($\text{Au}_1\text{Pd}_4@\text{SiTi}$). Interestingly the performances of the monometallic Au and Pd samples (Table 3, Entries 8 and 9 respectively) were low and close to that of the Pd-rich $\text{Au}_1\text{Pd}_4@\text{SiTi}$ sample. Very low activity was observed for the supported catalysts (Table 3, Entries 4–6). Moreover, important differences in FDCA selectivity were also observed. Indeed, the $\text{Au}_4\text{Pd}_1@\text{SiTi}$ sample (Figure 6) was much more selective to FDCA after 24 h than the two other samples (Figure 6a). A conversely higher selectivity to HFCA was observed for $\text{Au}_1\text{Pd}_1@\text{SiTi}$ (Figure 6a). Almost no FDCA formation was observed for the supported materials (Figure 6b). In contrast to the embedded samples, the FDC was the main product formed in the case of the supported catalysts.

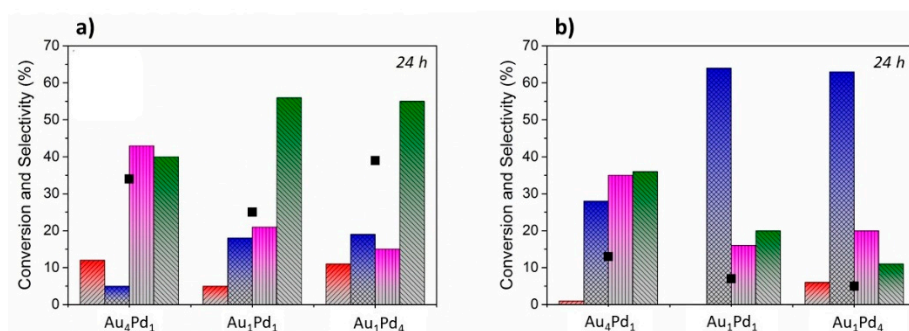


Figure 6. HMF oxidation in the aqueous phase in the absence of a base using (a) embedded and (b) supported catalysts; black—conversion, selectivity to: red—FDCA, blue—FDC, pink—HFCA, green—FFCA. Aqueous solution of HMF (30 μmol), substrate/metal = 18 (mol/mol), O_2 (1 bar), 100 $^\circ\text{C}$, 600 rpm.

As the total metal content was similar for all samples, the activity in the case of embedded catalysts was strongly affected by the composition of the alloyed nanoparticles, which is in good agreement with data earlier reported [20].

2.2. Furfural Oxidation

Catalytic tests for furfural oxidation using Au, Pd and AuPd–titanosilicate catalysts were performed using air as an oxidant at high pressure (26 bar). The results showed that the catalysts were also able to oxidize furfural to furoic acid (FA) in the absence of a base (Table 4). However, in all cases, the carbon balance was quite low (Table 4). This could be explained by the degradation of furfural on the acid supports and/or the adsorption of furfural on the SiTi matrix.

The results presented in Table 4 highlight the synergistic effect of Au_xPd_y bimetallic catalysts compared to their monometallic Au and Pd counterparts. Au_4Pd_1 and Au_1Pd_1 were the most active samples, although the former led to a higher yield of FA. The $\text{Au}_4\text{Pd}_1@\text{SiTi}$ catalyst presented a slightly higher performance (expressed in TON) than other compositions, which is also in good agreement with the HMF oxidation results presented above.

The effect of the stabilizing agent on catalytic activity was also evaluated when comparing Au, Pd and AuPd NPs stabilized with PVA and citrate (Table 4, Entry 9). The tests revealed no difference in activity, which means that both stabilizers were efficient in inducing an active catalytic formulation. No significant differences in mean particle sizes were observed for both stabilizers (*ca.* 3.8 nm with citrate and 4.1 nm with PVA). As observed above, a higher catalytic efficiency was achieved with $\text{Au}_x\text{Pd}_y@\text{SiTi}$ catalysts when compared to $\text{Au}_x\text{Pd}_y/\text{SiTi}$ supported catalysts (Table 4) for producing FA at higher yields. The exception was the $\text{Au}_4\text{Pd}_1/\text{SiTi}$ catalyst, which has led to 50% of the FA yield; however, when considering the TON rates, embedded catalysts were more efficient (Table 4). It is important to highlight the efficiency of these titanosilicate-based catalysts when compared to titanium

and zirconium catalysts (Table 4, Entries 10 and 11), as was already the case in HMF oxidation (Table 3). The latter achieved complete conversion in 10 h of reaction but showed low selectivity to FA. A blank test for the 2 h reaction showed a furfural conversion of 23%, selectivity to FA of 0%, carbon balance = 77%, and a conversion of 52% after 10 h of reaction, selectivity to FA of 0% and a carbon balance of 48% (Table 4, Entry 12). In the absence of a catalyst, it is not possible to obtain furoic acid, nor when using pure titanosilicate, although some conversion was observed. Apparently, some degradation through the formation of humins and humic acids occurred, considering that no other probable product was detected. This could also explain the low carbon balance values observed for the catalysts, since adsorption tests were performed and excluded the possibility of adsorption of FA or furfural in the pores and/or surface of the catalyst.

Table 4. Oxidation of furfural in the absence of a base for 10 h using embedded $\text{Au}_x\text{Pd}_y\text{@SiTi}$ and supported $\text{Au}_x\text{Pd}_y\text{/SiTi}$, Au/TiO_2 , Au/ZrO_2 catalysts. (Conditions: Aqueous solution of furfural (49.4 μmol), substrate/metal = 50 (mol/mol), air (26 bar), 110 °C, 600 rpm, ^a samples calcined at 500 °C).

Entry	Catalyst	C Balance %	S _{FA} %	X%	Y _{FA} %	TON
1	$\text{Au}_4\text{Pd}_1\text{@SiTi}$	54	45	83	37	91
2	$\text{Au}_1\text{Pd}_1\text{@SiTi}$	47	30	77	23	80
3	$\text{Au}_1\text{Pd}_4\text{@SiTi}$	58	23	54	12	57
6	$\text{Au}_4\text{Pd}_1\text{/SiTi}$	49	48	99	48	50
7	$\text{Au}_1\text{Pd}_1\text{/SiTi}$	56	18	54	10	28
8	$\text{Au}_1\text{Pd}_4\text{/SiTi}$	66	11	38	4	19
9	$\text{Au}_1\text{Pd}_{1\text{PVA}}\text{@SiTi}$	48	41	87	36	44
10	Au/TiO_2	8	8	100	8	43
11	Au/ZrO_2	37	32	92	29	45
12	blank	48	0	52	0	-
13	Au@SiTi	80	32	30	10	15
14	Pd@SiTi	73	20	34	7	17
15 ^a	$\text{Au}_4\text{Pd}_1\text{@SiTi}_{\text{cal}}$	38	2	63	1	-
16 ^a	$\text{Au}_1\text{Pd}_1\text{@SiTi}_{\text{cal}}$	86	12	16	2	-
17 ^a	$\text{Au}_1\text{Pd}_4\text{@SiTi}_{\text{cal}}$	12	1	88	1	-

3. Discussion

Embedded systems exhibit a higher level of intermolecular interaction between embedded metallic nanoparticles and the oxide from the titanosilicate matrix as compared to classical oxide-supported metal nanoparticles. The synthesis method presented herein to produce embedded catalysts allows us to maintain high metal dispersion during utilization, even for relatively high metal contents. The degree of metal support interactions could be controlled, resulting in different stabilization mechanisms. Embedded metal nanoparticle catalysts present a covalent link between preformed AuPd nanoparticles (citrate or PVP method of preparation) and the growing support. This allows better thermal and chemical stability and also enables us to tune the selectivity in catalytic oxidation reactions as well as obtaining interesting yields even without base addition. Indeed, monometallic Au and Pd catalysts showed very low activity in the oxidation of furfural and HMF. This is in good agreement with the literature data. The activity of monometallic catalysts in base free oxidation is generally low due to the adsorption of products on the metal surface, impeding the conversion of the substrates into the final products. Up to now only Au supported on basic oxides such as MgO, CuO or hydrotalcites reached high reaction yields. This is due to the partial leaching of the support and in situ base formation, as discussed in [21].

Several oxidation steps occur during the aerobic oxidation of HMF. Moreover, all these steps could occur simultaneously (Figure 5). Depending on the active metal used for the reaction, the oxidation to FDCA could proceed through the formation of HFCA or FDC. The mechanism of the HMF oxidation follows two pathways: (1) in the first step, the aldehyde group is oxidized to carboxylic group to form 5-hydroxymethyl-2-furancarboxylic acid (HFCA). In the second step, the 5-formyl-2-furancarboxylic

acid (FFCA) is formed due to the alcohol group oxidation to aldehyde; or (2) the hydroxyl group is oxidized to an aldehyde to form 2, 5-diformylfuran (FDC), and, in the second step, the oxidation of carbonyl group gives a monoacid: 5-formyl-2-furancarboxylic acid (FFCA). The FDCA is formed through oxidation of the aldehyde group of FFCA. It is well known that the reaction medium and catalyst composition govern the reaction pathway. Under high pH conditions (<7) the first pathway is favored, especially when gold-based catalysts are used [22]. As the oxidation of the alcohol group is the rate-determining step in the case of gold-based catalysts, the HFCA formation is generally favored. Casanova et al. [23] reported the formation of HFCA as the only intermediate detected on Au/TiO₂ and Au/CeO₂ catalysts in the HMF oxidation in basic medium. According to these authors, this might be due to the fast conversion of FFCA to FDCA. The formation of HFCA in basic medium is favored because of the aldehyde group, which can rapidly undergo hydration to a geminal diol. The further step, β -hydride elimination of the geminal diol to form a carboxylic acid, is also favored at a high pH by the OH[−] adsorbed on the metal surface. FDC and FFCA intermediate formation in base-free oxidation of HMF using AuPd/CNT catalyst was observed by Wang et al. [24]. The authors observed that the hydroxyl group oxidation was much faster than the aldehyde group. For the Au/CNT, the aldehyde group was oxidized, forming HFCA, as was also observed for the Au-based catalysts in basic medium (Au/CeO₂ and Au/TiO₂). However, in this case, the ring-opening reaction of HFCA occurred, forming side products. In the case of monometallic Pd and AuPd bimetallic catalysts the reaction pathway changed. The formation of FDC was observed, as Pd seems to facilitate the oxidation of the alcohol group. In addition, the rapid oxidation of FFCA to FDCA was favored in the case of the Pd samples. This is one of the limiting steps over gold-based catalysts under base-free conditions.

In order to confirm the base-free conditions during the furfural and HMF oxidation, pH measurements were performed during the reaction, as shown in Table 5. The furfural and HMF solutions are already acidic, showing a pH of 3.96 and 4.25, respectively.

Table 5. Final pH values of furfural and HMF oxidation reactions using embedded Au_xPd_y@SiTi and supported Au_xPd_y/SiTi catalysts.

Catalyst	Furfural		HMF	
	2 h	10 h	2 h	10 h
blank test	-	2.93	-	3.04
Au ₄ Pd ₁ @SiTi	3.81	3.36	3.93	2.55
Au ₁ Pd ₁ @SiTi	3.89	3.22	3.28	2.60
Au ₁ Pd ₄ @SiTi	3.74	3.69	3.30	2.93
Au ₄ Pd ₁ /SiTi	-	2.78	-	2.53
Au ₁ Pd ₁ /SiTi	-	3.73	-	3.20
Au ₁ Pd ₄ /SiTi	-	3.55	-	3.49
Au@SiTi	-	3.21	-	3.30
Pd@SiTi	-	3.34	-	3.41

The low pH observed due to acid formation after the oxidation reactions did not increase the leaching of the metals to the solution (which was confirmed by ICP analysis). Considering that the reactions occurred in an acidic medium, lower reaction rates are justified when compared to the reactions performed in a neutral or alkaline medium [20,25]. This means that the concept for the development of catalysts for reactions in aqueous medium in the absence of a base was successful, although the search for an increase in catalytic efficiency for these systems remains topical.

To benchmark the results obtained under base-free conditions, tests in the presence of a base were also conducted. The results are given in Table 6.

Table 6. Catalytic results obtained in the oxidation of HMF in the presence of the base. Conditions: Aqueous solution of HMF (30 μ mol), substrate/metal = 18 (mol/mol), O₂ (1 bar), 100 °C, 600 rpm, 2 molar equivalents of K₂CO₃ were added to the reactant solution before catalytic test.

Entry	Catalyst	Base	X%	Selectivity (%)			
				FDCA	FDC	HFCA	FFCA
1	Au ₄ Pd ₁ @SiTi	2 eq	37	3	14	34	49
2	Au ₁ Pd ₁ @SiTi	2 eq	18	4	30	37	29
3	Au ₁ Pd ₄ @SiTi	2 eq	4	3	34	53	10
4	Au ₄ Pd ₁ /SiTi	2 eq	34	2	15	32	51
5	Au ₁ Pd ₁ /SiTi	2 eq	5	8	15	60	17
6	Au ₁ Pd ₄ /SiTi	2 eq	5	9	14	59	18

The HMF conversion was much lower in the case of Au₄Pd₁@SiTi sample in the presence of a base (37%) as compared to base-free conditions (Table 3, Entry 1). However, the selectivity to FDCA was much higher (17%) in the reaction carried out without the base as compared to that in basic conditions (3%). In both cases, the activity of the catalysts was affected by the Au–Pd ratio. The monometallic catalysts showed very low oxidation activity of both molecules.

The activity of the catalysts was strongly affected by the calcination at 500 °C, as can be seen from Tables 3 and 4. For the Au₄Pd₁@SiTi_{cal} calcined sample, the selectivity to furoic acid decreased from 45% to 2%. The selectivity to FDCA reached only 1% instead of 22% for the non-calcined material (Table 3). The decrease in the activity is due to the collapse of the structure and suppression of the porosity of the material (decrease of the BET surface after calcination from 78 m²/g to 2 m²/g in the case of Au₄Pd₁ sample). These results are comparable to that observed for the bare support. As the metal particles are embedded into the matrix and the pores are blocked, there is no contact between the substrate and the metal. The conversion is due to the furfural and HMF degradation.

In these reactions, the highest activity was observed for Au₄Pd₁ compositions (Section 2.1, Figure 2b), which is in good agreement with the previous data. Indeed, the arrangement between gold and palladium atoms plays a crucial role in catalytic performances of the bimetallic catalytic systems [26,27]. Therefore, the optimization and control of the fine bimetallic nanoparticles structure constitute the major objective to obtain high catalytic performances (the so-called “catalysis by design”), which finally allows the design of the most effective catalytic materials. The synthesis protocol used for bimetallic nanoparticle preparation strongly affects the type of the catalyst morphology. The interaction between two metals strongly influences the catalytic performance, as already reported [28–30]. The optimal metal-to-metal ratio must be determined for a given reaction. In the case of bimetallic catalysts based on AuPd systems, the remarkable increase in the catalytic oxidation activity was already observed [31–36]. In liquid phase oxidation of aldehydes and alcohols, the AuPd nanoparticles have already proved to be twice as efficient as the Au or Pd alone. It has been proposed that Au plays the role of an electronic promoter of Pd [35,36], which is in good agreement with the observed core-shell structure. A compositional effect has also been reported, where a gradual increase in catalytic activity was observed with the increase in Pd content. An optimal Au–Pd molar ratio of about 1:1.86 was reported for gas phase CO oxidation [37]. In our case, the catalytic activity also passes through the maximum for Au₄Pd₁ composition. This is also in good agreement with the literature for liquid phase oxidation of glucose and benzyl alcohol [20,25]. It could be stated that an optimum ratio between Pd⁰ and Pd²⁺ species is necessary to maintain the high activity of these catalysts, as well to obtain high selectivity to desired products [20,38].

4. Materials and Methods

4.1. Materials

Chloroauric acid trihydrate ($\text{HAuCl}_4 \cdot 3\text{H}_2\text{O}$, 99.9%, Sigma-Aldrich (St. Louis, MO, USA)), sodium borohydride (NaBH_4 , 98%, Sigma-Aldrich (St. Louis, MO, USA)), poly(vinyl alcohol) (PVA, Sigma-Aldrich (St. Louis, MO, USA), MW 55,000 g/mol), sodium citrate ($\text{Na}_3\text{C}_6\text{H}_5\text{O}_7$, 99%, Sigma-Aldrich (St. Louis, MO, USA)), furfural ($\text{C}_5\text{H}_4\text{O}_2$, >99%, Sigma-Aldrich (St. Louis, MO, USA)), 5-hydroxymethylfurfural (HMF, 99%, Sigma-Aldrich (St. Louis, MO, USA)), furoic acid (FA, 99% Sigma-Aldrich (St. Louis, MO, USA)), 5-hydroxymethyl-2-furancarboxylic acid (HMFA, >99%, Sigma-Aldrich (St. Louis, MO, USA)), 2, 5-diformylfuran (DFF, >99%, Sigma-Aldrich (St. Louis, MO, USA)), 5-formyl-2-furoic acid (FFCA, >99%, Sigma-Aldrich (St. Louis, MO, USA)), 2, 5-furandicarboxylic acid (FDCA, 99%, Sigma-Aldrich (St. Louis, MO, USA)) were of analytical grade and were used as received. Deionized water (18.2 M Ω) was used for the preparation of all the needed solutions.

4.2. Synthesis of Au, Pd and AuPd Titanosilicate Catalysts

In 200 mL of water with vigorous stirring, Au and Pd precursors (HAuCl_4 solution 30 wt.% and PdCl_2 , 10.11×10^{-5} mol of metal) and 2 mL of a sodium citrate solution (0.17 M, metal:citrate = 1:3.4) were added. Then, a freshly prepared solution of NaBH_4 (50 mM, 10 mL, NaBH_4/Au (mol/mol) = 5) was then added drop by drop to form a metallic sol; the color of the sol was dark brown (Au_1Pd_1 , Au_1Pd_4) and light-red (Au, Au_4Pd_1). After 20 min of sol generation, 400 mL of water were added. Then, 10 mL of a solution containing titanium isopropoxide (TIP) and (3-aminopropyl)triethoxysilane (APTES) (Si:Ti (mol/mol) = 3:2) were filtered using a 0.22 μm filter membrane and slowly added. After the hydrolysis of the oxide precursors (2 h), the slurry was filtered, the solid washed with ethanol (2×25 mL) and dried at room temperature (RT) for 24 h.

4.3. Synthesis of Au, Pd and AuPd Supported Catalysts

ZrO₂- and TiO₂- supported catalysts were prepared by the sol-immobilization method described in [21]. SiTi support used for the immobilization of bimetallic AuPd nanoparticles was synthesized similarly to the method described above. In the standard procedure, the preformed AuPd nanoparticles were put into contact with the SiTi support in water for 2 h under stirring. After this, the solid was removed by centrifugation, washed with ethanol and dried in air for 24 h.

4.4. Catalytic Reactions

Base-free oxidation of furfural: catalytic reactions under air atmosphere were performed using the Freeslate MultiReactor available on EQUIPEX platform REALCAT. It consisted of 24 parallel batch reactors for high throughput screening, in which each reactor was loaded with an aqueous furfural solution (2 mL, 24.7 mmol L⁻¹) and the Au-based catalyst (*ca.* 10 mg, 0.9 μmol Au). The reaction was carried out at 20 bar of air (26 bar final pressure), 110 °C, 600 rpm, 2 h (SPR reactions). Base free oxidation of HMF: catalytic reactions under O₂ atmosphere were performed using a 50 mL Fischer-Porter loaded with an aqueous HMF solution (2 mL, 30 μmol) and the Au-based catalyst (*ca.* 100 mg). The reaction was carried out at 1 bar of O₂, 100 °C, 600 rpm, with different reaction times, from 0.5 h to 24 h. In both cases, after the reaction the catalyst was removed by filtration, the products were diluted in water and analyzed. The analysis of the products was performed by UHPLC chromatography using the Aminex HPX-87H Ion Exclusion (Agilent (Santa Clara, CA, USA)) column for the analysis of furfural oxidation. Formic acid (0.5% *v/v*) was used as a mobile phase at a flowrate of 0.30 mL/min and product formation was observed on a UV-VIS detector/photodiode array detector at 253 nm. For the analysis of HMF oxidation products, a Phenomenex (Torrance, CA, USA) column (ROA, organic acid H⁺; 300 \times 7.8 mm) was used. Sulphuric acid (5 mmol/L) was used as a mobile phase at a flowrate of 0.60 mL/min and the products were detected on a Shodex RI-101 detector at 265 nm.

4.5. Characterization

TEM electron microscopy images were recorded by placing a drop of the particle's dispersion in ethanol over a carbon film supported on a copper grid. The samples were studied using a FEI Titan Themis 60–300 microscope (FEI, Hillsboro, OR, USA). The average Au nanoparticle size was determined, taking into account at least 300 particles. X-ray photoelectron spectroscopy (XPS) experiments were performed with K-alpha surface analysis (Thermo Scientific (Waltham, MA, USA)) equipment with an Al-K α X-ray source (1486.6 eV) and a flood gun. The investigated area was approximately circular (approx. 300 μm in diameter) and three different areas of each sample were examined. The binding energy (BE) of the spectra was corrected with that of adventitious carbon C1s (C–C, C–H) at 284.8 eV. Nitrogen adsorption and desorption analysis was performed using a TriStar II Plus analyzer (Micromeritics (Norcross, GA, USA)). The samples were subjected to a pretreatment before the analyses to eliminate impurities that were adsorbed onto the surface. Namely, the samples were heated up to 150 $^{\circ}\text{C}$ with a temperature ramp of 10 $^{\circ}\text{C min}^{-1}$ and then maintained at this temperature for 60 min under vacuum. To determine the total surface area of the analysed catalysts the BET (Brunauer–Emmett–Teller) model was used. The pore volume was also calculated using the BJH (Barrett–Joyner–Halenda) method. ICP-OES (inductively coupled plasma optical emission spectrometry) analysis was performed using Agilent 720-ES ICP-OES (Santa Clara, CA, USA) equipment combined with the Vulcan 42S automated digestion system. The digestion procedure of the samples prior to analysis was as follows; first, 10 mg of catalysts were weighted and then 500 μL HF and 1.5 mL of aqua regia were distributed in sample holder (Polypropylene tube) by the syringe robot. Then, the tubes were heated up to 65 $^{\circ}\text{C}$ overnight. All samples were neutralized and diluted up to 20 mL with ultrapure water prior to analysis. XRF (M4 Tornado) analysis was performed using an Energy Dispersive X Ray Fluorescence (EDXRF) spectrometer provided from Bruker (Billerica, MA, USA). This spectrometer is equipped with X-ray Rhodium tube and the beam is micro-focused using a polycapillary lens enabling excitation of an area of 200 μm . The measurement was done under vacuum (20 mbar). The X-ray generator was operated at 50 kV and 200 μA and different filters were used to reduce the background (100 μm Al/50 μm Ti/25 μm Cu). Quantitative analysis was done using the fundamental parameter (FP) (standardless).

5. Conclusions

Bimetallic AuPd embedded systems were developed and applied in the furfural and HMF base-free oxidation reactions. The catalysts consisted of AuPd nanoparticles embedded in a titanasilicate support. In this embedded catalyst, as shown above, the effect of AuPd bimetallic nanoparticles (obtained by citrate stabilization) coupled with the specific properties of the support resulted in an efficient catalyst for the oxidation of both molecules in an aqueous medium and in the absence of a homogenous base. The results shown in this article highlight the advantages of Au and AuPd catalysts for the selective oxidation of biomass-derived substrates, such as HMF and furfural, in the absence of a base. The $\text{Au}_x\text{Pd}_y\text{@SiTi}$ catalysts were effective for the oxidation of furfural and HMF to their respective FA and FDCA acids in the absence of a base, reaching 99% and 89% of conversion, respectively, after 10 h of reaction. The catalyst based on bimetallic AuPd NPs surrounded by a titanasilicate matrix allowed the production of the corresponding acids more efficiently than the monometallic versions of Au and Pd (Au@SiTi and Pd@SiTi) or, even, their supported versions (Au/SiTi , Pd/SiTi and AuPd/SiTi). No catalyst leaching was detected (Au, Ti, Si); in fact, the entire reaction occurred in acid medium (initial and final pH <4), allowing the isolation of FA and FDCA directly from the reaction medium after reaction took place. This type of catalyst could also be applied for the oxidation of other alcohols and aldehydes in base-free conditions.

Author Contributions: Conceptualization, C.P.F., L.M.R. and R.W.; methodology, J.T.-R.; N.J.S.C. and C.W.L.; writing—original draft preparation, C.P.F.; R.F. and R.W.; writing—review and editing, C.P.F.; R.W.; E.T.-N.; Â.A.T.-N.; L.M.R. and F.D.; visualization, N.J.S.C.; M.T.M. and R.F.; supervision, R.W. and L.M.R.; project administration, C.P.F. and L.M.R.; funding acquisition, L.M.R. All authors have read and agreed to the published version of the manuscript.

Funding: This research was funded by Fundação de Amparo à Pesquisa do Estado de São Paulo (FAPESP), grant number 2014/10824-3 2017/03235-0, 2014/15159-8.

Acknowledgments: The authors acknowledge Gustavo Saraiva Silveira for the help with figures and drawings and CNPq for the support. The REALCAT platform benefits from a state subsidy administrated by the French National Research Agency (ANR) within the frame of the ‘Investments for the Future’ program (PIA), with the contractual reference ‘ANR-11-EQPX-0037’. The European Union, through the FEDER funding administered by the Hauts-de-France Region, has co-financed the platform. Centrale Lille, CNRS, and the University of Lille as well as the Centrale Initiatives Foundation, are thanked for their financial contributions to the acquisition and implementation of the equipment of the REALCAT platform. Chevreul Institute (FR 2638), Ministère de l’Enseignement Supérieur, de la Recherche et de l’Innovation, Hauts-de-France Region and FEDER are acknowledged for supporting and funding partially this work. We also acknowledge CNPEM for the FEI Titan Themis 60–300 microscope use and LNNano for XPS measurements.

Conflicts of Interest: The authors declare no conflict of interest.

References

- Chheda, J.N.; Huber, G.W.; Dumesic, J.A. Liquid-Phase Catalytic Processing of Biomass-Derived Oxygenated Hydrocarbons to Fuels and Chemicals. *Angew. Chem. Int. Ed.* **2007**, *46*, 7164–7183. [\[CrossRef\]](#)
- Corma, A.; Iborra, S.; Velty, A. Chemical Routes for the Transformation of Biomass into Chemicals. *Chem. Rev.* **2007**, *107*, 2411–2502. [\[CrossRef\]](#)
- Davis, S.E.; Ide, M.S.; Davis, R.J. Selective oxidation of alcohols and aldehydes over supported metal nanoparticles. *Green Chem.* **2013**, *15*, 17–45. [\[CrossRef\]](#)
- Dumeignil, F.; Capron, M.; Katryniok, B.; Wojcieszak, R.; Löfberg, A.; Girardon, J.-S.; Desset, S.; Araque-Marin, M.; Jalowiecki-Duhamel, L.; Paul, S. Biomass-derived Platform Molecules Upgrading through Catalytic Processes: Yielding Chemicals and Fuels. *J. Jpn. Pet. Inst.* **2015**, *58*, 257–273. [\[CrossRef\]](#)
- Li, X.; Jia, P.; Wang, T. Furfural: A Promising Platform Compound for Sustainable Production of C4 and C5 Chemicals. *ACS Catal.* **2016**, *6*, 7621–7640. [\[CrossRef\]](#)
- Aresta, M.; Dibenedetto, A.; Dumeignil, F. *Biorefineries an Introduction*; Walter de Gruyter GmbH & Co. KG: Berlin, Germany, 2015.
- Guimarães, L.H.S. Carbohydrates from Biomass: Sources and Transformation by Microbial Enzymes. In *Carbohydrates-Comprehensive Studies on Glycobiology and Glycotechnology*; Intech: London, UK, 2012; Volume 20, pp. 441–456.
- Zhang, Z.; Deng, K. Recent Advances in the Catalytic Synthesis of 2,5-Furandicarboxylic Acid and Its Derivatives. *ACS Catal.* **2015**, *5*, 6529–6544. [\[CrossRef\]](#)
- Zhu, Y.; Shen, M.; Xia, Y.; Lu, M. Au/MnO₂ nanostructured catalysts and their catalytic performance for the oxidation of 5-(hydroxymethyl)furfural. *Catal. Commun.* **2015**, *64*, 37–43. [\[CrossRef\]](#)
- Yang, B.; Dai, Z.; Ding, S.-Y.; Wyman, C.E. Enzymatic hydrolysis of cellulosic biomass. *Biofuels* **2011**, *2*, 421–449. [\[CrossRef\]](#)
- Besson, M.; Gallezot, P.; Pinel, C. Conversion of Biomass into Chemicals over Metal Catalysts. *Chem. Rev.* **2014**, *114*, 1827–1870. [\[CrossRef\]](#)
- Wojcieszak, R.; Cuccovia, I.M.; Silva, M.A.; Rossi, L.M. Selective oxidation of glucose to glucuronic acid by cesium-promoted gold nanoparticle catalyst. *J. Mol. Catal. A Chem.* **2016**, *422*, 35–42. [\[CrossRef\]](#)
- Biella, S.; Castiglioni, G.L.; Fumagalli, C.; Prati, L.; Rossi, M. Application of gold catalysts to selective liquid phase oxidation. *Catal. Today* **2002**, *72*, 43–49. [\[CrossRef\]](#)
- Delidovich, I.V.; Taran, O.P.; Matvienko, L.G.; Simonov, A.N.; Simakova, I.L.; Bobrovskaya, A.N.; Parmon, V.N. Selective Oxidation of Glucose over Carbon-supported Pd and Pt Catalysts. *Catal. Lett.* **2010**, *140*, 14–21. [\[CrossRef\]](#)
- Liu, C.; Zhang, J.; Huang, J.; Zhang, C.; Hong, F.; Zhou, Y.; Li, G.; Haruta, M. Efficient Aerobic Oxidation of Glucose to Gluconic Acid over Activated Carbon-Supported Gold Clusters. *ChemSusChem* **2017**, *10*, 1976–1980. [\[CrossRef\]](#) [\[PubMed\]](#)

16. Miedziak, P.J.; Alshammari, H.; Kondrat, S.A.; Clarke, T.J.; Davies, T.E.; Morad, M.; Morgan, D.J.; Willock, D.J.; Knight, D.W.; Taylor, S.H.; et al. Base-free glucose oxidation using air with supported gold catalysts. *Green Chem.* **2014**, *16*, 3132–3141. [\[CrossRef\]](#)
17. Suchomel, P.; Kvitek, L.; Pucek, R.; Panacek, A.; Halder, A.; Vajda, S.; Zboril, R. Simple size-controlled synthesis of Au nanoparticles and their size-dependent catalytic activity. *Sci. Rep.* **2018**, *8*, 4589. [\[CrossRef\]](#) [\[PubMed\]](#)
18. Lolli, A.; Albonetti, S.; Utili, L.; Amadori, R.; Ospitali, F.; Lucarelli, C.; Cavani, F. Insights into the reaction mechanism for 5-hydroxymethylfurfural oxidation to FDCA on bimetallic Pd-Au nanoparticles. *Appl. Catal. A Gen.* **2015**, *504*, 408–419. [\[CrossRef\]](#)
19. Lilga, M.A.; Hallen, R.T.; Gray, M. Production of oxidized derivatives of 5-hydroxymethylfurfural (HMF). *Top. Catal.* **2010**, *53*, 1264–1269.
20. Wojcieszak, R.; Ferraz, C.P.; Jin Sha, J.; Houda, S.; Rossi, L.M.; Paul, S. Advances in Base-Free Oxidation of Bio-Based Compounds on Supported Gold Catalysts. *Catalysts* **2017**, *7*, 352. [\[CrossRef\]](#)
21. Ferraz, P.C.; Zieliński, M.; Pietrowski, M.; Heyte, S.; Dumeignil, F.; Rossi, L.M.; Wojcieszak, R. Influence of Support Basic Sites in Green Oxidation of Biobased Substrates Using Au-Promoted Catalysts. *ACS Sustain. Chem. Eng.* **2018**, *6*, 16332–16340. [\[CrossRef\]](#)
22. Ishida, T.; Kinoshita, N.; Okatsu, H.; Akita, T.; Takei, T.; Haruta, M. Influence of the Support and the Size of Gold Clusters on Catalytic Activity for Glucose Oxidation. *Angew. Chem. Int. Ed.* **2008**, *120*, 9405–9408. [\[CrossRef\]](#)
23. Casanova, O.; Iborra, S.; Corma, A. Biomass into Chemicals: Aerobic Oxidation of 5-Hydroxymethyl-2-furfural into 2,5-Furandicarboxylic Acid with Gold Nanoparticle Catalysts. *ChemSusChem* **2009**, *2*, 1138–1144. [\[CrossRef\]](#) [\[PubMed\]](#)
24. Wan, X.; Zhou, C.; Chen, J.; Deng, W.; Zhang, Q.; Yang, Y.; Wang, Y. Base-Free Aerobic Oxidation of 5-Hydroxymethyl-furfural to 2,5-Furandicarboxylic Acid in Water Catalyzed by Functionalized Carbon Nanotube-Supported Au-Pd Alloy Nanoparticles. *ACS Catal.* **2014**, *4*, 2175–2185. [\[CrossRef\]](#)
25. Sha, J.; Paul, S.; Dumeignil, F.; Wojcieszak, R. Au-based bimetallic catalysts: How the synergy between two metals affects their catalytic activity. *RSC Adv.* **2019**, *9*, 29888–29901. [\[CrossRef\]](#)
26. Ferrer, D.; Torres-Castro, A.; Gao, X.; Sepúlveda-Guzmán, S.; Ortiz-Méndez, U.; José-Yacamán, M. Three-layer core/shell structure in Au-Pd bimetallic nanoparticles. *Nano Lett.* **2007**, *7*, 1701–1705. [\[CrossRef\]](#) [\[PubMed\]](#)
27. Mu, R.; Fu, Q.; Xu, H.; Zhang, H.; Huang, Y.; Jiang, Z.; Zhang, S.; Tan, D.; Bao, X. Synergetic effect of surface and subsurface Ni species at Pt-Ni bimetallic catalysts for CO oxidation. *JACS* **2011**, *133*, 1978–1986. [\[CrossRef\]](#) [\[PubMed\]](#)
28. Benkó, T.; Beck, A.; Frey, K.; Srankó, D.F.; Geszti, O.; Sáfrán, G.; Maróti, B.; Schay, Z. Bimetallic Ag-Au/SiO₂ catalysts: Formation, structure and synergistic activity in glucose oxidation. *Appl. Catal. A Gen.* **2014**, *479*, 103–111. [\[CrossRef\]](#)
29. Heidkamp, K.; Aytemir, M.; Vorlop, K.-D.; Prüße, U. Ceria supported gold-platinum catalysts for the selective oxidation of alkyl ethoxylates. *Catal. Sci. Technol.* **2013**, *3*, 2984–2992. [\[CrossRef\]](#)
30. Comotti, M.; Pina, C.D.; Rossi, M. Mono- and bimetallic catalysts for glucose oxidation. *J. Mol. Catal. A Chem.* **2006**, *251*, 89–92. [\[CrossRef\]](#)
31. Silva, T.A.G.; Teixeira-Neto, E.; López, N.; Rossi, L.M. Volcano-like behavior of Au-Pd core-shell nanoparticles in the selective oxidation of alcohols. *Sci. Rep.* **2014**, *4*, 5766. [\[CrossRef\]](#)
32. Enache, D.I.; Edwards, J.K.; Landon, P.; Solsona-Espriu, B.; Carley, A.F.; Herzing, A.A.; Watanabe, M.; Kiely, C.J.; Knight, D.W.; Hutchings, G.J. Solvent-Free oxidation of primary alcohols to aldehydes using Au-Pd/TiO₂ Catalysts. *Science* **2006**, *311*, 362–365. [\[CrossRef\]](#)
33. Dimitratos, N.; Villa, A.; Wang, D.; Porta, F.; Su, D.; Prati, L. Pd and Pt catalysts modified by alloying with Au in the selective oxidation of alcohols. *J. Catal.* **2006**, *244*, 113–121. [\[CrossRef\]](#)
34. Ketchie, W.C.; Murayama, M.; Davis, R.J. Selective oxidation of glycerol over carbon-supported AuPd catalysts. *J. Catal.* **2007**, *250*, 264–273. [\[CrossRef\]](#)
35. Kesavan, L.; Tiruvalam, R.; Rahim, M.H.A.; bin Saiman, M.I.; Enache, D.I.; Jenkins, R.L.; Dimitratos, N.; Lopez-Sanchez, J.A.; Taylor, S.H.; Knight, D.W.; et al. Solvent-free oxidation of primary carbon-hydrogen bonds in toluene using Au-Pd alloy nanoparticles. *Science* **2011**, *331*, 195–199. [\[CrossRef\]](#) [\[PubMed\]](#)

36. Silva, T.A.G.; Landers, R.; Rossi, L.M. Magnetically recoverable AuPd nanoparticles prepared by a coordination capture method as a reusable catalyst for green oxidation of benzyl alcohol. *Catal. Sci. Technol.* **2013**, *3*, 2993–2999. [[CrossRef](#)]
37. Pritchard, J.; Kesavan, L.; Piccinini, M.; He, Q.; Tiruvalam, R.; Dimitratos, N.; Lopez-Sanchez, J.A.; Carley, A.F.; Edwards, J.K.; Kiely, C.J.; et al. Direct synthesis of hydrogen peroxide and benzyl alcohol oxidation using Au–Pd catalysts prepared by sol immobilization. *Langmuir* **2010**, *26*, 16568–16577. [[CrossRef](#)]
38. Silva, T.A.G.; Ferraz, C.; Gonçalves, R.V.; Teixeira-Neto, E.; Wojcieszak, R.; Rossi, L.M. Restructuring of gold-palladium alloyed nanoparticles: A step towards more active catalysts for oxidation of alcohols. *ChemCatChem* **2019**, *11*, 4021–4027. [[CrossRef](#)]



© 2020 by the authors. Licensee MDPI, Basel, Switzerland. This article is an open access article distributed under the terms and conditions of the Creative Commons Attribution (CC BY) license (<http://creativecommons.org/licenses/by/4.0/>).